

Ultra-Wideband Dual-Polarized Patch Antenna with Four Capacitively Coupled Feeds

Fuguo Zhu, Steven Gao, *Member, IEEE*, Anthony TS Ho, *Senior Member, IEEE*, Raed A. Abd-Alhameed, *Senior Member, IEEE*, Chan H. See, Tim WC Brown, *Member, IEEE*, Jianzhou Li, Gao Wei, and Jiadong Xu

Abstract — A novel dual-polarized patch antenna for ultra-wideband (UWB) applications is presented. The antenna consists of a square patch and four capacitively coupled feeds to enhance the impedance bandwidth. Each feed is formed by a vertical isosceles trapezoidal patch and a horizontal isosceles triangular patch. The four feeds are connected to the microstrip lines that are printed on the bottom layer of the grounded FR4 substrate. Two tapered baluns are utilized to excite the antenna to achieve high isolation between the ports and reduce the cross-polarization levels. In order to increase the antenna gain and reduce the backward radiation, a compact surface mounted cavity is integrated with the antenna. The antenna prototype has achieved an impedance bandwidth of 112% at $(|S_{11}| \leq -10 \text{ dB})$ whereas the coupling between the two ports is below -28 dB across the operating frequency range. The measured antenna gain varies from 3.91 to 10.2 dBi for port 1 and from 3.38 to 9.21 dBi for port 2, with a 3-dB gain bandwidth of 107%.

Index Terms — UWB antenna, dual-polarized antenna, patch antenna, capacitively coupled feed, surface mounted cavity

I. INTRODUCTION

UWB communication system has attracted increasing attention due to its advantages of high speed data rate and low spectral power density, since the Federal Communications Commission (FCC) first approved the frequency range from 3.1 to 10.6 GHz for commercial UWB applications in 2002 [1]. This has increased the demands on the UWB systems and subsequently to stimulate the research activities in various UWB antenna designs [2-3]. Moreover, dual-polarized UWB antennas are more attractive compared with linearly polarized antennas, as the channel capacity is significantly enhanced due to the polarization

diversity technique. The performance of imaging/radar systems can also be improved by employing dual-polarized UWB antennas [4-5]. Challenges of dual-polarized UWB antenna designs include wide impedance matching, high isolation between two polarization ports, low cross-polarization, stable radiation performance across the wide bandwidth, and low-cost.

Microstrip patch antennas have been widely applied in wireless communication systems mainly owing to their characteristics of low-profile, low-cost and easy fabrication. However, a single-layer patch antenna usually operates over a limited frequency range only which can't satisfy the bandwidth requirements for UWB applications. Consequently, several techniques have been proposed in the literature to extend the bandwidth of dual-polarized patch antennas. For example, one typical technique is the use of various probe-fed mechanisms, such as printed Γ -shaped probe [6], L-shaped probe [7-8], meandered-line probe [9] and hook-shaped probe [10]. Another approach is to employ stacked patches with capacitive-probe feed [11], proximity feed [12] and aperture-coupled feed [13-17]. Alternatively, the bandwidth can be increased by embedding slots in the patch [18-20]. Other techniques include the hybrid feed technique such as L-shaped probe & aperture-coupled feed [21], gap-coupled feed & aperture-coupled feed [22], and meandered strip & aperture-coupled feed [23], and employing electromagnetic-fed method [24]. Recently, broadband dual-polarized magneto-electric dipole antennas with differential-feed have been proposed in [25-26].

Initially, compared with probe-fed patch antennas [6-12], aperture-coupled stacked-patch antennas [13-17] can be easily integrated with active RF circuits and to achieve high polarization purity but high backward radiation. To increase the front-to-back ratio and reduce the backward radiation, a reflector patch can be employed below the feed to enhance the desired performance [15-17]. Hybrid feed patch antennas can achieve high isolation and low cross-polarization while two ports may have different radiation characteristics. In contrast to hybrid feed method, differential-feed technique has been utilized in dual-polarized patch antennas as it can enhance the port isolation and reduce cross-polarization levels as shown in [7-8, 10, 19-20, 25-26]. To summarize and compare some of the state-of-the-art work in wideband

F. Zhu and S. Gao are with the School of Engineering and Digital Arts, University of Kent, CT2 7NZ, UK. (zhu.fuguo@hotmail.com; s.gao@kent.ac.uk).

A. TS Ho is with the Department of Computing, University of Surrey, Guildford, GU2 7XH, UK (A.Ho@surrey.ac.uk).

R. A. Abd-Alhameed is with Antennas and Applied Electromagnetics Research Group, University of Bradford, Bradford, BD7 1DP, UK (r.a.a.abd@bradford.ac.uk).

C. H. See is with the Engineering, Sports, and Sciences (ESS) Academic Group, University of Bolton, BL3 5AB, UK. (chs1@bolton.ac.uk)

T. W. C. Brown is with Centre for Communication Systems Research, University of Surrey, Guildford, GU2 7XH, UK (T. Brown@surrey.ac.uk)

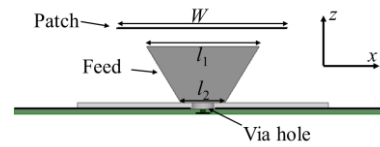
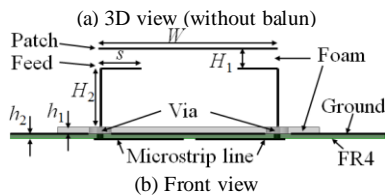
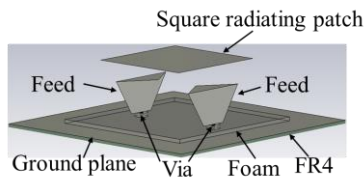
J. Z. Li, G. Wei and J. D. Xu are with Northwestern Polytechnical University, Xi'an, 710072, P.R. China.

dual-polarized patch antenna designs, Table 1 lists the performances in terms of operational bandwidth (BW) and port isolation among the previously mentioned designs. As can be observed in Table 1, a few dual-polarized patch antennas can achieve over 50% bandwidth [16, 25-26] but they are unable to cover the whole UWB band (3.1-10.6 GHz). Thus, the objective of this work is to design a low-cost dual-polarized patch antenna which can operate over 3.1-10.6 GHz with high isolation, low cross-polarization levels and stable radiation patterns.

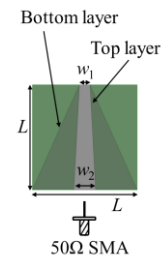
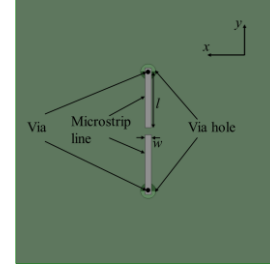
Table 1 Performance of different dual-polarized patch antennas.

Ref.	BW (%)	Isolation (dB)	Ref.	BW (%)	Isolation (dB)	Ref.	BW (%)	Isolation (dB)
[6]	24.9	29	[13]	20.9	36	[20]	31	35
[7]	23.8	30	[14]	24.4	30	[21]	27	25
[8]	29	30	[15]	39	35	[22]	14	40
[9]	26	25	[16]	52	39	[23]	14	40
[10]	37	40	[17]	33	16	[24]	38.7	40
[11]	30	NaN	[18]	19	28	[25]	65.9	36
[12]	17	15	[19]	46.5	38	[26]	68	36

In this paper, a dual-polarized patch antenna capacitively coupled through four feeds is proposed. Compared with other dual-polarized patch antennas reported, the bandwidth of the proposed antenna is significantly increased and an impedance bandwidth of over 110% is obtained by applying such feeding mechanism. In order to realize a differential feed, the dual-polarized patch antenna is excited by two tapered baluns, thus achieving a high isolation (better than 28 dB) and the cross-polarization levels are reduced. Relatively stable radiation patterns and consistent gain performance have been achieved when employing a surface mounted cavity. After including the cavity, the obtained 3-dB gain bandwidth is as large as 107%. The structure of this paper will be divided into three sections after the introduction. In section II, the proposed antenna structure and step-by-step design procedures and concepts will be elucidated. Section III is devoted to describe the simulated and measured results of the proposed antennas while section IV is used to draw a conclusion on the findings of this work.



(c) Side view



(d) Bottom layer of the grounded FR4 substrate (e) Tapered balun [27].
Fig. 1 Configuration of the proposed single-polarized UWB antenna with capacitively coupled feed.

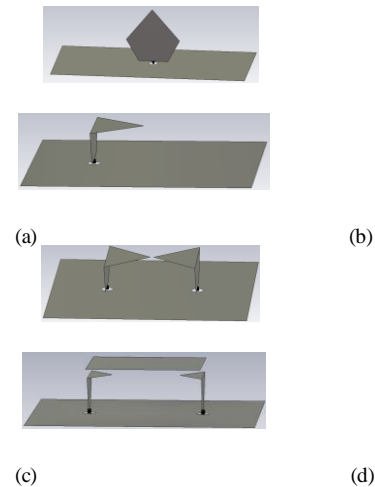


Fig. 2 (a)-(d) Evolution procedure from a monopole antenna to the proposed UWB antenna (balun is not shown).

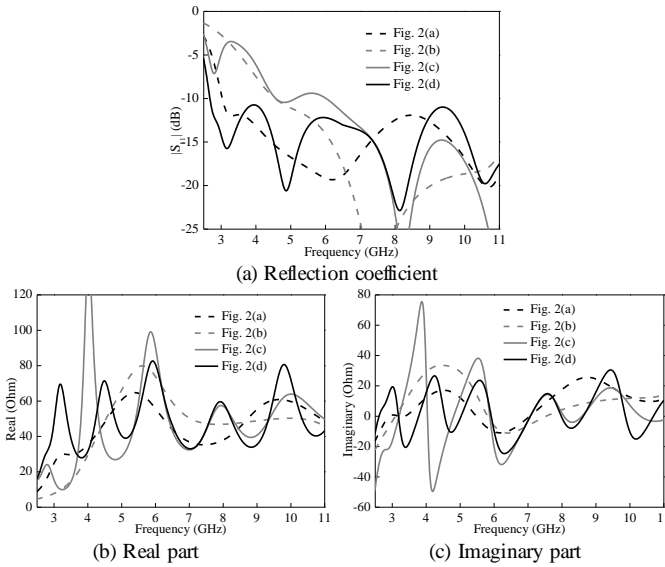


Fig. 3 Simulated (a) reflection coefficient and (b), (c) input impedance of the proposed antenna in the design evolution process from Figs. 2(a)-(d).

II. ANTENNA GEOMETRY AND DESIGN CONCEPTS

The antenna design procedure starts by designing a single-polarized UWB antenna. Fig. 1 presents the configuration of the proposed single-polarized UWB antenna. The square radiating patch with a side length of W is supported by a Rohacell foam of relative permittivity $\epsilon_1 = 1.03$ and thickness $H_1 = 3$ mm, and capacitively excited by two identical feeds which are symmetrically located with respect to the center of the antenna. Each feed consists of two portions, i.e., the vertical part is an isosceles trapezoidal patch and the horizontal part is an isosceles triangular patch. The horizontal and vertical patches share the same length l_1 . The square ground plane with a size of $60 \text{ mm} \times 60 \text{ mm}$, is printed on the top layer of an FR4 substrate ($\epsilon_2 = 4.55$, $h_2 = 0.8$ mm) and two identical microstrip lines with a length of l and a width of w are on the other side. The characteristic impedance of the microstrip line is designed to be 50Ω . A Rohacell foam with thickness of $h_1 = 1$ mm is inserted between the ground plane and the bottom side of the capacitively coupled feed. It will have little effect after removing the foam layer. The outer ends of the two microstrip lines are connected to the capacitively coupled feeds by two vias through via holes which are embedded in the ground plane. Good impedance matching across a wide frequency range can be obtained by selecting proper dimensions of the capacitively coupled feeds. To realize a differential feed which can lead to low cross-polarization and high isolation, a simple tapered balun [27] which could operate

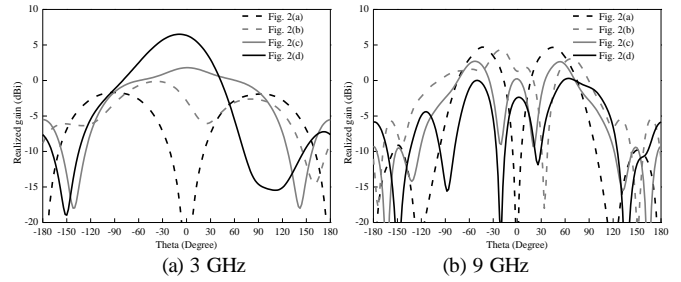


Fig. 4 Simulated co-polarized radiation patterns in the yz plane at 3 and 9 GHz.

from 3 to 10 GHz, is utilized to excite the antenna. To achieve good impedance matching, the characteristic impedance of the twin line is set to 100Ω . As shown in Fig. 1(e), the balun is printed on a 1.6 mm thick FR4 substrate and perpendicularly placed to the surface of the grounded FR4 substrate. The top sides of the balun are connected to the inner ends of two microstrip lines while the bottom side is soldered to a 50Ω SMA connector. It is worth mentioning that the gap between the inner ends of the two microstrip lines is the same as the thickness of the FR4 substrate for the balun.

To understand the basic operating principle of the antenna, Figs. 2(a)-(d) show the detailed design evolution from a basic monopole to the proposed UWB antenna while Figs. 3(a)-(c) illustrate the corresponding reflection coefficient and input impedance of each antenna configuration. This analysis starts by considering a basic monopole which is composed of a trapezoidal patch and a triangular patch vertically mounted above a ground plane as shown in Fig. 2(a). It is well known that this antenna can operate over a wide frequency band and the height of the antenna is about a quarter-wavelength at the lowest operating frequency ($f_{L_{2(a)}}$) [28]

$$f_{L_{2(a)}} \approx \frac{c}{4 \times (s + H_2)} \quad (1)$$

where c and $f_{L_{2(a)}}$ are the speed of light in free space and the lowest operating frequency, $s = 13$ mm and $H_2 = 10$ mm are the heights of the triangular patch and trapezoidal patch, respectively. The calculated $f_{L_{2(a)}}$ using Eq. (1) is 3.2 GHz which is close to the simulated value of 3 GHz at $|S_{11}|$ better than -10 dB. As illustrated in Fig. 3(a), the $|S_{11}|$ of the basic monopole in Fig. 2(a) is below -10 dB from 3 to 11 GHz. To physically realize the operation of this antenna, the variations of the input impedance plot are also given in Figs. 3(b) and (c). As can be seen, the antenna exhibits three resonances at 3, 5.4 and 7 GHz with optimum 50Ω impedance matching at 4.5, 6.2 and 8.7 GHz. By gathering these closely spaced resonant modes, the desired broad bandwidth of this antenna can be attained [29]. Furthermore, Fig. 4 presents the simulated co-polarized radiation patterns of this antenna in yz plane at 3 and 9 GHz. At 3 GHz, the maximum radiation of this monopole is along the ground plane while the radiation

is shifted above the ground plane at 9 GHz and the main lobe becomes narrower.

In order to achieve directional pattern and reduce the overall height of the antenna, the vertical triangular patch is bent to be parallel to the ground plane, as shown in Fig. 2(b). This has shortened the height from 23 to 10 mm which corresponds to a reduction of 56.5%. However, this modification impairs the impedance matching at lower operating band and shifts the lowest operating frequency to 4.4 GHz due to the coupling between the triangular patch and the ground plane, as observed in Fig. 3(a). To further investigate this, Figs. 3(b) and (c) show that, the change of the structure has slight effect on the imaginary part of the input impedance while the real part in the band from 3 to 4 GHz is significantly reduced, which deteriorates the impedance matching. As expected, the folded monopole has directional radiation though the maximum radiation at 3 GHz is off boresight and pointed at -30° . The pattern can be regarded as the contribution of the vertical patch and the horizontal patch, as the maximum radiation of the vertical patch is along the ground plane and the horizontal patch has broadside radiation, as shown in Fig. 4.

In order to enhance the maximum radiation focus on the broadside direction and reduce the cross-polarization level through the differential feed technique, another identical antenna element is added and mirrored into the antenna structure, as illustrated in Fig. 2(c). As can be noticed in Fig. 3(a), the lowest operating frequency of the differential-fed folded monopole is shifted down to 3 GHz while the reflection coefficient in the low band is larger than -10 dB. The input impedance in Figs. 3(b) and (c) show four series resonances (3.25 GHz, 4.85 GHz, 7 GHz, 8.8 GHz) and four parallel resonances (4 GHz, 5.9 GHz, 8 GHz, 10 GHz). As can be observed, the real and imaginary parts have large fluctuations in the low band, which indicates poor impedance matching. Scrutinizing the pattern plot in Fig. 4 with this configuration, the main beam of this antenna is along broadside at 3 GHz though the side lobe levels are higher than the main beam at 9 GHz. This is caused by various electrical lengths between the vertical patches at different frequencies.

The final stage of the design process is to introduce a parasitic patch to achieve good impedance matching over the UWB band, as shown in Fig. 2(d) and Fig. 3. The proposed antenna is similar as the L-shaped probe-fed patch antenna [7, 29] while the L-probe is replaced by the L-shaped patch and the impedance bandwidth is significantly enhanced. The following formulas [29] are employed to predict the lowest operating frequency ($f_{L-2(d)}$) of the patch antenna in Fig. 2(d)

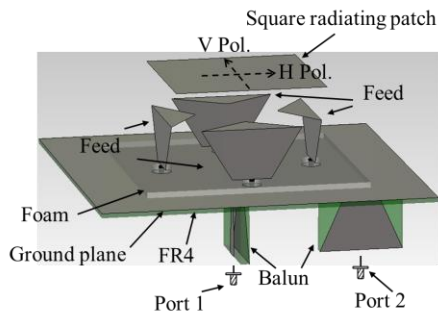
$$f_{L-2(d)} \approx \frac{c}{2(W + 2\Delta W)\sqrt{\epsilon_{er}}} \quad (2)$$

$$\Delta W \approx 0.412 \frac{(\epsilon_{er} + 0.3)\left(\frac{W}{H_t} + 0.264\right)}{(\epsilon_{er} - 0.258)\left(\frac{W}{H_t} + 0.813\right)} H_t \quad (3)$$

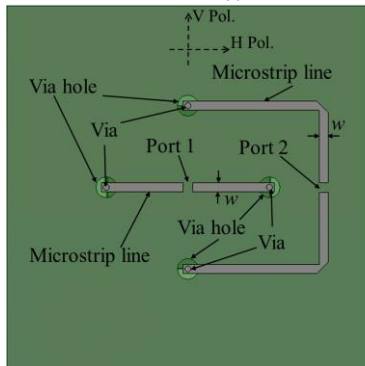
$$H_t = H_1 + H_2 + h_1 \quad (4)$$

where ϵ_{er} is the effective dielectric constant and is selected as unity in this design. ΔW is the resonance edge extension of the patch and H_t is the distance between the patch and the ground plane. The initial values of the dimensions are: $W=27$ mm, $H_1=3$ mm, $H_2=9$ mm and $h_1=1$ mm. The corresponding predicted $f_{L-2(d)}$ using Eq. (2-4) is 3.5 GHz. The discrepancy between the predicted value and the simulated value at 3 GHz can be attributed to the coupling between the triangular patches and the square radiating patch. As indicated in Fig. 3(a), the proposed single-polarized antenna can operate over a wide frequency band covering the frequency range from 3 to 11 GHz for $|S_{11}| \leq -10$ dB. Moreover, as noticed in Figs. 3(b) and (c), introducing the parasitic patch to the antenna structure does not alter the resonant modes of the antenna in Fig. 2(c), however it provides a stable impedance response with less variation values of resistance (30 to 80 Ohm) and reactance (-20 to 30 Ohm) over the operating frequency band. To understand the contribution of this structure into the radiation pattern, Fig. 4 describes the patterns at 3 and 9 GHz. As can be clearly seen, the antenna has more directional pattern compared to the antenna structure in Fig. 2(c) at 3 GHz. It should be noted that although the proposed antenna and the designs in [7] and [30] have used L-shaped feeds, the design processes are different. The antennas in [7] and [30] are developed from traditional narrowband patch antennas. The bandwidths of the antennas in [7] and [30] are increased due to the use of the L-shaped feed while the initial idea to use L-shaped feed in the proposed antenna is to achieve directional radiation. Moreover, compared with antennas in [7] and [30], the bandwidth of the proposed antenna is significantly increased.

The performance of the tapered balun has been investigated as it affects the overall performance of the differential-fed antenna. It is found that the insertion loss of the tapered balun is less than 2 dB and the reflection coefficient is less than -10 dB over 3 to 11 GHz band; including the phase difference of the balanced ports over the same band is almost $\pm 180^\circ$ with relative phase errors around $\pm 5^\circ$. These results can confirm that the tapered balun is appropriate for feeding the proposed UWB antenna.



(a) 3D view



(b) Bottom layer of the grounded FR4 substrate

Fig. 5 Configuration of the proposed dual-polarized UWB antenna.

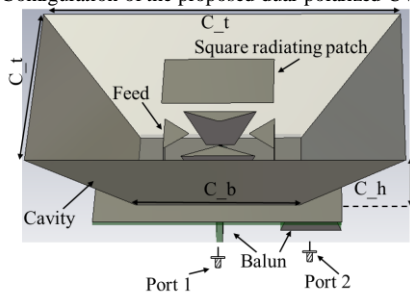


Fig. 6 Configuration of the cavity-backed dual-polarized UWB antenna



(a)

(b)

Fig. 7 Photos of the fabricated dual-polarized UWB patch antennas. (a) without a cavity and (b) with a cavity

A. Dual-polarized UWB antenna design

Based on the analysis of the single-polarized UWB antenna in the previous section, a dual-polarized UWB antenna with dual orthogonal linear polarization can be realized by adding another pair of capacitively coupled feeds. The added feeds are also connected to two identical L-shaped microstrip lines with a length of 34.45 mm. As shown in Fig. 5(a), four identical capacitively coupled feeds are placed symmetrically with respect to the center of the antenna and used to excite a single square radiating patch. The four feeds are connected to four microstrip lines by vias through via holes in the ground plane. The microstrip lines have the same width and printed on the bottom layer of the grounded FR4 substrate, as shown in Fig. 5(b). In order to realize a differential feed, two baluns are soldered to the two pair of microstrip lines respectively, with port 1 for achieving horizontal polarization and port 2 for achieving vertical polarization.

B. Cavity-backed dual-polarized UWB antenna

To further reduce the side lobe and increase the antenna gain, a surface mounted cavity is employed in the antenna. As shown in Fig. 6, the compact inverted pyramidal cavity with a square cross section occupies a volume of $C_t \times C_t \times C_h$ mm³. It has a height of C_h and the side lengths of its top and bottom sections are C_t and C_b , respectively. It should be noted that the cavity-backed dual-polarized UWB antenna has the same antenna parameters (patch, capacitively coupled feed, ground and balun) as the antenna proposed in the previous section. The purpose of using a cavity is to increase the antenna gain at higher frequencies while not deteriorating the wide impedance matching. To determine the geometric parameters, the effects on the impedance matching and the radiation patterns have been studied. The study has found that the antenna gain can be increased by increasing the height of the cavity and reducing the size of cross section, while the

increment of the height and reduction of the length will deteriorate the impedance matching. The optimized values of the parameters for achieving high gain while maintain good impedance matching are $C_h = 23$ mm, $C_t = 90$ mm and $C_b = 40$ mm.

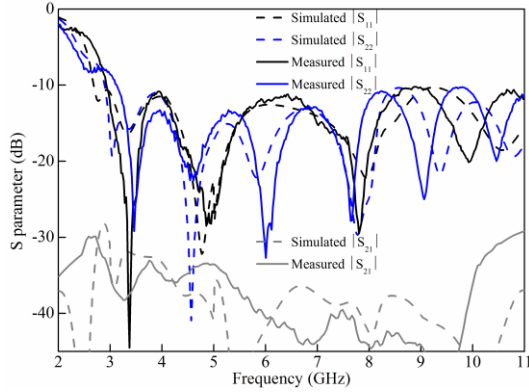


Fig. 8 Simulated and measured reflection coefficient and mutual coupling for the antenna without a cavity. Antenna parameters are: $W = 27$ mm, $H_1 = 3$ mm, $H_2 = 9$ mm, $h_1 = 1$ mm, $h_2 = 0.8$ mm, $s = 6$ mm, $l_1 = 18$ mm, $l_2 = 7$ mm, $l = 12.7$ mm, $w = w_1 = 1.5$ mm, $L = 15$ mm and $w_2 = 3.1$ mm.

III. RESULTS AND DISCUSSION

To validate the design concept, the dual-polarized UWB patch antennas without and with the cavity have been constructed and tested. The photos of the prototypes are shown in Fig. 7. The simulated and measured results of reflection coefficient and mutual coupling for the dual-polarized UWB patch antenna without a cavity are shown in Fig. 8. It is observed that, the simulated impedance bandwidths ($|S_{11}| \leq -10$ dB) are 121.4% (from 2.69 to 11 GHz) and 117% (from 2.88 to 11 GHz) at port 1 and port 2 respectively, while the measured impedance bandwidths ($|S_{11}| \leq -10$ dB) are 116.1% (from 2.92 to 11 GHz) and 112.1% (from 3.1 to 11 GHz), respectively. These discrepancies at lower frequencies are mainly attributed to two aspects. The first is caused by the tapered balun which is not strictly balanced and the other is the ground plane which has a small electrical dimension at low frequencies. The overlapped impedance bandwidths over port 1 and port 2 at the criterion ($|S_{11}| \leq -10$ dB) in simulation and measurement are 117% (from 2.88 to 11 GHz) and 112.1% (from 3.1 to 11 GHz), respectively. It is also found that the simulated and measured mutual coupling is less than -30 dB over the whole operating frequency band.

Fig. 9 presents the measured radiation patterns in two principal planes for the antenna without cavity. As observed, port 1 and port 2 have almost similar radiation characteristics. The slight asymmetry in the back lobe for port 2 is mainly owing to the asymmetrical positions of the two baluns. The patterns in the H-plane are stable and have similar beamwidths within the whole frequency band. The levels of side lobes in the E-plane increase and the beamwidth becomes narrower as the antenna operates at higher frequencies. The cross-polarization levels in the

broadside direction are less than -15 dB. At 9 GHz, the slight increment of cross-polarization level in the H-plane is observed. The simulated and measured antenna gain versus frequency for the antenna without a cavity is shown in Fig. 10. The peak gains are 7.28 dBi at 3 GHz for port 1 and 6.42 dBi at 3.5 GHz for port 2, respectively. It is noticed that the antenna gain varies from 7.28 to 0.19 dBi at port 1 and from 6.42 to -0.56 dBi at port 2. The electrical length between the vertical patches of the feeds varies against frequency, thus leading to higher side lobe levels at higher frequencies. Hence, the boresight gain drop is observed in the frequency band. It is also noted that, the measured result is lower than the simulation, which is mainly due to the dielectric loss of FR4.

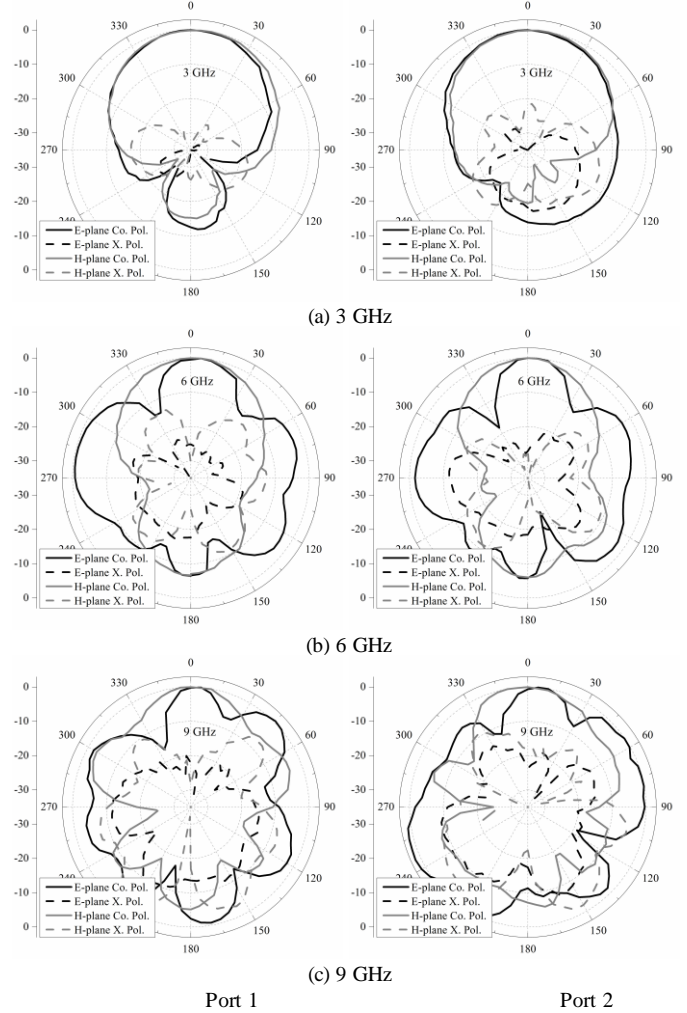


Fig. 9 Measured co- and cross-polarized radiation patterns in two principal planes for the antenna without a cavity. Left: port 1 is excited and port 2 is terminated with 50 Ω . Right: port 2 is excited and port 1 is terminated with 50 Ω .

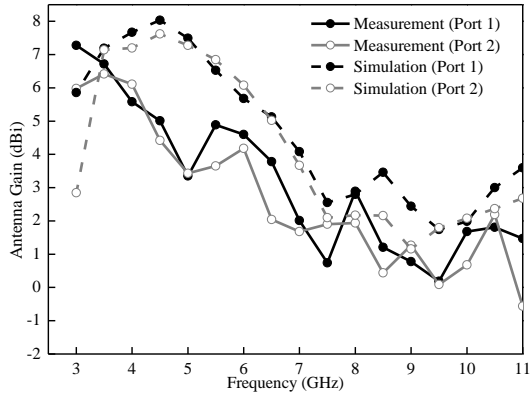


Fig. 10 Simulated and measured antenna gain for port 1 and port 2.



Fig. 11 Two identical antennas positioned face to face.

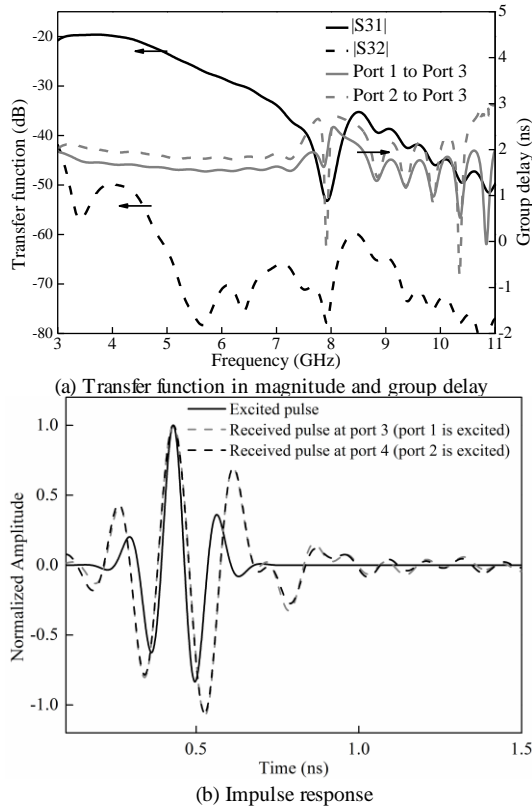


Fig. 12 (a) Transfer function in magnitude and group delay, and (b) Impulse response of the antenna without a cavity.

In order to fully characterize this UWB antenna, the following section is given to understand the ability of distortionless pulse transmission for the dual-polarized UWB patch antenna without a cavity. The setup is shown in Fig. 11, in which two identical antennas are located face to face. In this case, Antenna 1 is excited for transmitting signal and Antenna 2 is for receiving the pulse. The corresponding ports of Antenna 2 are denoted as port 3 and port 4. It is also noted that port 1 and port 3 have the same polarization while port 2 and port 4 have the same polarization. The Gaussian

pulse is adopted from [31] and covers the wide bandwidth from 3.1 to 10.6 GHz. Fig. 12(a) displays the magnitude of the transfer function. As observed, magnitude of the transfer function between the ports with the same polarization ($|S_{31}|$) is much larger than $|S_{32}|$. The value of $|S_{31}|$ varies from -20 to -50 dB while $|S_{32}|$ changes from -40 to -80 dB due to the co- and cross-polarization. A null is also observed at 8 GHz. Moreover, group delay of the proposed antenna is examined and also shown in Fig. 12 (a). It is defined as the negative derivative of the phase for the transfer function. As can be observed, the group delay varies from 0 to 3 ns over the desired frequency band. Fig. 12(b) presents the received pulse at port 3 when port 1 is excited and received pulse at port 4 when port 2 is excited. The received pulse can be obtained by applying the Inverted Fast Fourier Transform (IFFT) from the product of the transmission coefficient and the frequency response of the excited pulse or from the model in CST Microwave Studio. The null in the magnitude or nonlinear phase of the transfer function may cause the distortion of the excited pulse. All the pulses are normalized and synchronized for comparison. As indicated, the waveforms of the received pulses are not identical with those of excited pulses and slightly ringing effect is observed. However, the waveforms within the peaks have similar shape. The fidelity between the excited and received pulses can be estimated using a correlation of the waveforms in the time domain. The fidelity factor is computed and found to be around 62% which indicates that the received pulse is only distorted which can be corrected by choosing a proper template.

The performance of the antenna with a cavity has also been measured. The simulated and measured results of reflection coefficient and mutual coupling are shown in Fig. 13. As observed, the impedance matching over a wide frequency band is not deteriorated due to the presence of the cavity. The simulated impedance bandwidths ($|S_{11}| \leq -10$ dB) are 121.4% (from 2.69 to 11 GHz) and 116% (from 2.9 to 11 GHz) at port 1 and port 2 respectively, while the measured impedance bandwidths ($|S_{11}| \leq -10$ dB) are 113% (from 3.06 to 11 GHz) and 112% (from 3.1 to 11 GHz), respectively. The overlapped impedance bandwidths for port 1 and port 2 at definition $|S_{11}| \leq -10$ dB in simulation and measurement are 116% (from 2.9 to 11 GHz) and 112% (from 3.1 to 11 GHz), respectively. It is also found that the inclusion of the **cavity has little effect on the mutual coupling**. The measured mutual coupling is below -28 dB across the whole operating frequency range.

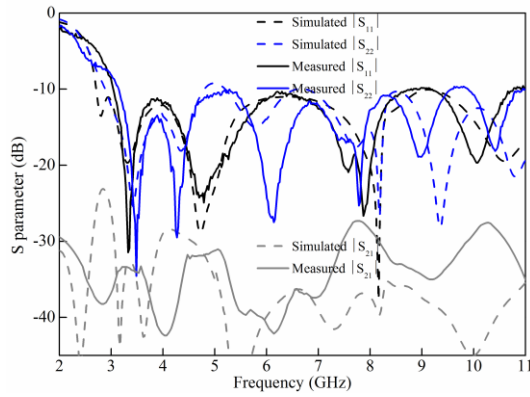


Fig. 13 Simulated and measured reflection coefficient and mutual coupling for the cavity-backed dual-polarized UWB antenna.

The measured radiation patterns for the cavity-backed antenna are illustrated in Fig. 14. It is noticed that, the levels of side lobes and backward radiation at high frequencies are significantly reduced due to the employment of the surface mounted cavity. The pattern characteristics at port 1 and port 2 are summarized in Table 2. For port 1, the F/B ratio reaches 24.7, 16, and 10.2 dB at 3, 6 and 9 GHz, respectively. The cross-polarization level increases slightly against frequency, with -20 dB at 3 GHz, -15.5 dB at 6 GHz and -9 dB at 9 GHz. The HPBW in the E-plane is narrower than that in the H-plane. The HPBW in the E-plane varies from 56° at 3 GHz, 26° at 6 GHz to 17° at 9 GHz. The HPBW in the H-plane decreases versus frequency, being 64° at 3 GHz, 43° at 6 GHz and 28° at 9 GHz. Port 2 has similar pattern characteristics as port 1. As observed, the F/B ratio at port 2 reaches 19, 17, and 10.7 dB at 3, 6 and 9 GHz, respectively. The cross-polarization level increases slightly against frequency, being -22 dB at 3 GHz, -14.3 dB at 6 GHz and -8 dB at 9 GHz. The HPBW in the E-plane is 57° at 3 GHz, 24° at 6 GHz and 16° at 9 GHz while in the H-plane it decreases slightly against frequency, being 63° at 3 GHz, 40° at 6 GHz and 30° at 9 GHz.

Fig. 15 presents the simulated and measured antenna gain for the cavity-backed dual-polarized UWB antenna. As illustrated, the gain performance for port 1 and port 2 is significantly increased and relatively consistent when the cavity is utilized. The antenna gain varies from 10.2 to 3.91 dBi at port 1 and from 9.21 to 3.38 dBi at port 2, respectively. The obtained 3-dB gain bandwidths for port 1 and port 2 are 112% (from 2.9 to 10.3 GHz) and 107% (from 3 to 10 GHz). The 3-dB gain bandwidth of the cavity-backed dual-polarized antenna is 107% (from 3 to 10 GHz).

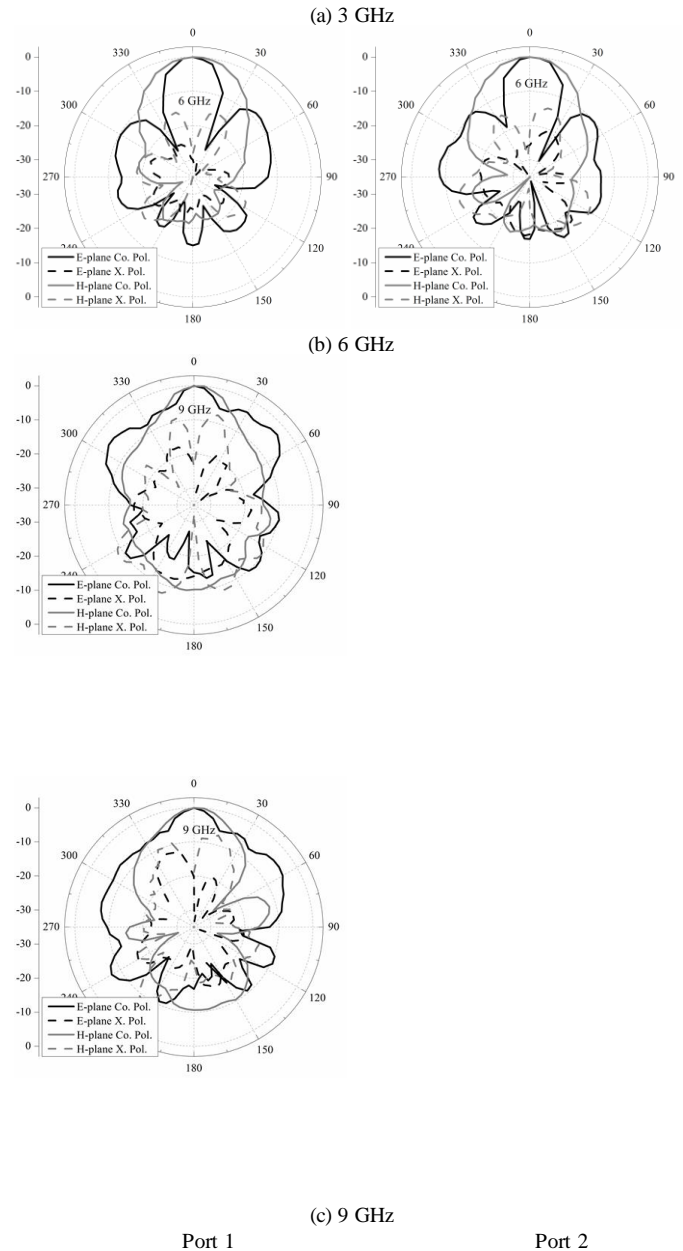
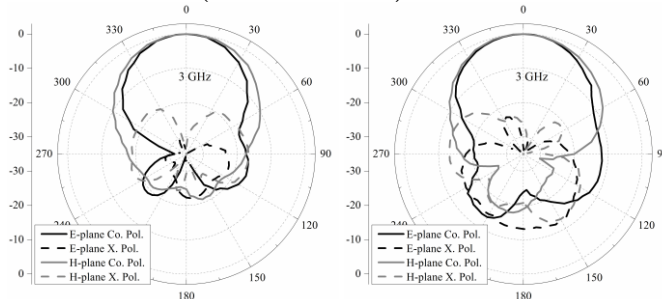


Fig. 14 Measured co- and cross-polarized radiation patterns for the cavity-backed dual-polarized UWB antenna.

Fig. 16 shows the transfer function in magnitude, group delay and impulse response of the antenna with a cavity. Compared with the antenna without a cavity, the magnitude of the transfer function between the ports with the same polarization ($|S_{31}|$) is significantly enhanced and varies from -10 to -35 dB. A null is also observed at 8 GHz and may cause distortion of the input signal. To further study this, the group delay across the operating frequency band is plotted. As noticed, the group delay varies from 1 to 4.5 ns with the largest value

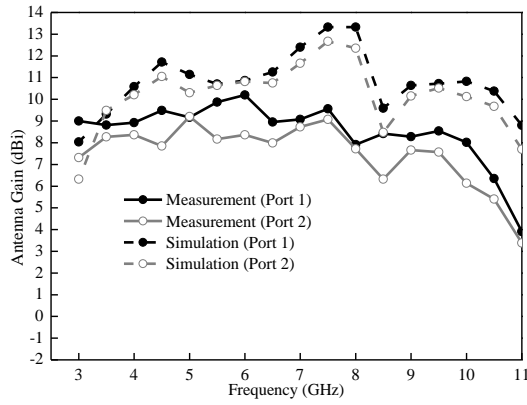
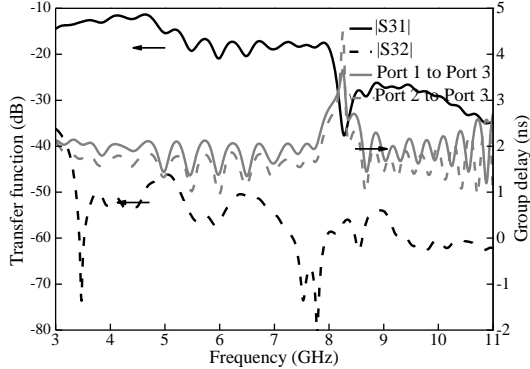
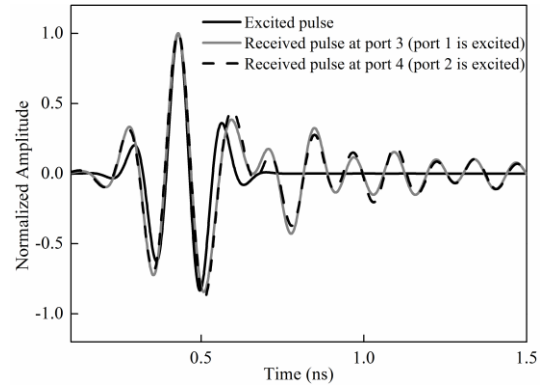


Fig. 15 Simulated and measured antenna gain for the cavity-backed antenna



(a) Transfer function in magnitude and group delay



(b) Impulse response

Fig. 16 (a) Transfer function in magnitude and group delay, and (b) Impulse response of the antenna with a cavity.

close to 8 GHz. This observation is caused due to the phase and pattern distortion and gain drop near 8 GHz, which is shown in Fig. 15. Fig. 16(b) shows the received pulse at port 3 when port 1 is excited and received pulse at port 4 when port 2 is excited. All the pulses are normalized and synchronized for comparison. The fidelity factor of the antenna reaches around 86%. Compared with the antenna without a cavity, the fidelity is increased by 24% after including the cavity.

Table 2 Summary of pattern characteristics for the cavity-back dual-polarized UWB antenna at 3, 6 and 9 GHz.

Frequency	port 1					port 2				
	Gain (dBi)	F/B ratio (dB)	X. pol. level (dB)	HPBW (°)		Gain (dBi)	F/B ratio (dB)	X. pol. level (dB)	HPBW (°)	
				E plane	H plane				E plane	H plane
3 GHz	9	24.7	-20	56	64	7.32	19	-22	57	63
6 GHz	10.2	16	-15.5	26	43	8.36	17	-14.3	24	40
9 GHz	8.28	10.2	-9	17	28	7.66	10.7	-8	16	30

F/B ratio is front-to-back ratio; HPBW is half-power beamwidth; X. pol. is cross-polarization.

IV. CONCLUSION

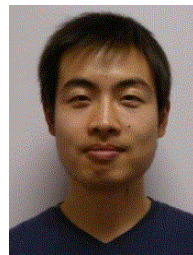
A novel dual-polarized UWB patch antenna excited by two tapered baluns has been presented. It consists of a square patch and four capacitively coupled feeds. The current distributions on the square patch at different frequencies have been studied for understanding the operating principle. Two antenna designs with a planar reflector or a surface mounted cavity have been designed, fabricated and tested. Compared with the antenna with a planar reflector, the cavity-backed patch antenna can operate over a wide frequency range with an impedance

bandwidth of 112%. The measured antenna gain ranges from 10.2 to 3.91 dBi and from 9.21 to 3.38 dBi for port 1 and port 2, respectively. The 3-dB gain bandwidth of up to 107.6% is achieved and the measured isolation is over 28 dB within the whole frequency band.

V. REFERENCES

- [1] P. Li, J. Liang, and X. D. Chen, "Study of printed elliptical/circular slot antennas for ultrawideband applications," *IEEE Trans. Antennas Propag.*, vol. 54, no. 6, 2006, pp. 1670-1675.
- [2] Z. N. Chen, M. J. Ammann, X. M. Qing, X. H. Wu, T. S. P. See, and A. L. Cai, "Planar antennas," *IEEE Microw. Mag.*, vol. 7, 2006, pp. 63-73.

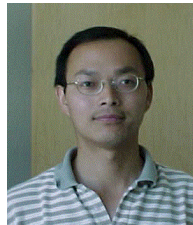
- [3] H. G. Schantz, "A brief history of UWB antennas," *IEEE A & E Syst. Mag.*, vol. 19, no. 4, 2004, pp. 22-26.
- [4] X. Li, G. Adamiuk, M. Janson, and T. Zwick, "Polarization diversity in ultra-wideband imaging systems," *2010 IEEE International Conference on Ultra-Wideband (ICUWB)*, vol. 1, pp. 1-4, 2010.
- [5] L. Zwirello, G. Adamiuk, W. Wiesbeck, and T. Zwick, "Measurement verification of dual-orthogonal polarized UWB monopulse radar system," *2010 IEEE International Conference on Ultra-Wideband (ICUWB)*, vol. 2, pp. 1-4, 2010.
- [6] L. Siu, H. Wong, and K. M. Luk, "A dual-polarized magneto-electric dipole with dielectric loading," *IEEE Trans. Antennas Propag.*, vol. 57, no. 7, 2009, pp. 616-623.
- [7] H. Wong, K. L. Lau, and K. M. Luk, "Design of dual-polarized L-probe patch antenna arrays with high isolation," *IEEE Trans. Antennas Propag.*, vol. 52, no. 1, 2004, pp. 45-52.
- [8] Y. X. Guo, K. W. Khoo, and L. C. Ong, "Wideband dual-polarized patch antenna with broadband baluns" *IEEE Trans. Antennas Propag.*, vol. 55, no. 1, 2007, pp. 78-83.
- [9] H. W. Lai and K. M. Luk, "Dual polarized patch antenna fed by meandering probes" *IEEE Trans. Antennas Propag.*, vol. 55, no. 9, 2007, pp. 2625-2627.
- [10] K. S. Ryn and A. A. Kishk, "Wideband dual-polarized microstrip patch excited by hook shaped probe," *IEEE Trans. Antennas Propag.*, vol. 56, no. 12, 2008, pp. 3645-3649.
- [11] J. Huang, Z. Hussein, and A. Petros, "A wide-band dual-polarized VHF microstrip antenna for global sensing of sea ice thickness," *IEEE Antennas and Propagation Society International Symposium*, vol. 2B, pp. 684-687, 2005.
- [12] J. L. Vazquez-Roy, V. Krozer, and J. Dall, "Wideband dual-polarization microstrip patch antenna array for airborne ice sounder," *IEEE Antennas Propag. Mag.*, vol. 54, no. 4, pp. 98-107, 2012.
- [13] S. Gao, L. W. Li, M. S. Leong, and T. S. Yeo, "Dual-polarized slot-coupled planar antenna with wide bandwidth," *IEEE Trans. Antennas Propag.*, vol. 51, no. 3, 2003, pp. 441-448.
- [14] S. Gao, L. W. Li, M. S. Leong, and T. S. Yeo, "A broad-band dual-polarized microstrip patch antenna with aperture coupling," *IEEE Trans. Antennas Propag.*, vol. 51, no. 4, 2003, pp. 898-900.
- [15] M. Barba, "A high-isolation, wideband and dual-linear polarization patch antenna," *IEEE Trans. Antennas Propag.*, vol. 56, no. 5, 2008, pp. 1472-1476.
- [16] K. Ghorbani and R. B. Waterhouse, "Dual polarized wide-band aperture stacked patch antennas," *IEEE Trans. Antennas Propag.*, vol. 52, no. 8, 2004, pp. 2171-2174.
- [17] A. A. Serra, P. Nepa, G. Manara, G. Tribellini, and S. Cioci, "A wide-band dual-polarized stacked patch antenna," *IEEE Antennas Wireless Propag. Lett.*, vol. 6, 2007, pp. 141-143.
- [18] R. C. Paryani, P. F. Wahid, and N. Behdad, "A wideband, dual-polarized, substrate-integrated cavity-backed slot antenna," *IEEE Antennas Wireless Propag. Lett.*, vol. 9, 2010, pp. 645-648.
- [19] B. Li, Y. Z. Yin, W. Hu, Y. Ding, and Y. Zhao, "Wideband dual-polarized patch antenna with low cross polarization and high isolation," *IEEE Antennas Wireless Propag. Lett.*, vol. 11, 2012, pp. 427-430.
- [20] S. G. Zhou, P. K. Tan, and T. H. Chio, "Low-profile, wideband dual-polarized antenna with high isolation and low cross polarization," *IEEE Antennas Wireless Propag. Lett.*, vol. 11, 2012, pp. 1032-1035.
- [21] Y. X. Guo, K. M. Luk, and K. F. Lee, "Broadband dual polarization patch element for cellular-phone base stations," *IEEE Trans. Antennas Propag.*, vol. 50, no. 2, 2002, pp. 251-253.
- [22] T. W. Chiou and K. L. Wong, "Broad-band dual-polarized single microstrip patch antenna with high isolation and low cross polarization," *IEEE Trans. Antennas Propag.*, vol. 50, no. 3, 2002, pp. 399-401.
- [23] C. Y. D. Sim, C. C. Chang, and J. S. Row, "Dual-fed dual-polarized patch antenna with low cross polarization and high isolation," *IEEE Trans. Antennas Propag.*, vol. 57, no. 10, 2009, pp. 3405-3409.
- [24] J. J. Xie, Y. Z. Yin, J. H. Wang, and X. L. Liu, "Wideband dual-polarised electromagnetic-fed patch antenna with high isolation and low cross-polarisation," *Electron. Lett.*, vol. 49, no. 3, 2013, pp. 171-173.
- [25] B. Q. Wu and K. M. Luk, "A broadband dual-polarized magneto-electric dipole antenna with simple feeds," *IEEE Antennas Wireless Propag. Lett.*, vol. 8, 2009, pp. 60-63.
- [26] Q. Xue, S. W. Liao, and J. H. Xu, "A differentially-driven dual-polarized magneto-electric dipole antenna," *IEEE Trans. Antennas Propag.*, vol. 61, no. 1, 2013, pp. 425-430.
- [27] A. Mehdipour, K. M. Aghdam, M. R. K. Khatib, and R. F. Dana, "A practical feeder for differential elliptical antennas in ultra-wideband applications," *Microw. Opt. Technol. Lett.*, vol. 50, no. 8, pp. 2103-2107, 2008.
- [28] S. Y. Suh, W. L. Stutzman, and W. A. Davis, "A new ultrawideband printed monopole antenna: the planar inverted cone antenna (PICA)," *IEEE Trans. Antennas Propag.*, vol. 52, no. 5, 2004, pp. 1361-1365.
- [29] B. Allen, M. Dohler, E. E. Okon, W. Q. Malik, A. K. Brown, and D. J. Edwards, *Ultra-wideband Antennas and Propagation for Communications, Radar and Imaging*, John Wiley & Sons, 2007.
- [30] C. L. Mark, K. M. Luk, K. F. Lee, and Y. L. Chow, "Experimental study of a microstrip patch antenna with an L-shaped probe," *IEEE Trans. Antennas Propag.*, vol. 48, no. 5, 2000, pp. 777-783.
- [31] C. H. See, R. A. Abd-Alhameed, H. I. Hrag, N. J. McEwan, P. S. Excell, and J. M. Noras, "A low-profile ultra-wideband modified planar inverted-F antenna," *IEEE Trans. Antennas Propag.*, vol. 61, no. 1, 2013, pp. 100-108.



Fuguo Zhu was born in Jiangsu, China, in 1986. He received his M.Sc. degree in electromagnetic theory and microwave technology from Northwestern Polytechnical University, Xi'an, P.R. China, in 2011, and his Ph.D. degree in Electronic Engineering from the University of Kent, Canterbury, UK, in 2014.

He worked as a Ph.D. student at Surrey Space Centre, University of Surrey, Guildford, UK, from October 2010 to March 2013. His research interests include UWB antenna, dual-polarized UWB antenna,

and UWB antenna array.



Steven Gao (M'01) received the Ph.D. degree in microwave engineering from Shanghai University, Shanghai, China, in 1999. He is a Professor in antennas and microwave/millimeter-wave systems at University of Kent, UK. His research covers space antennas, smart antennas, phased arrays, millimeter-wave antennas, high-efficiency RF/microwave power amplifiers, satellite communications, UWB radars, synthetic-aperture radars, EM modeling and small satellites. He was a Senior Lecturer and Head of Space Antennas and Microwave System Group at Surrey Space Center, University of Surrey, UK.

He is General Chair of Loughborough Antennas and Propagation International Conference, UK, 2013. He is a co-editor of <<Space Antenna Handbook>> (Wiley, 2012), published over 160 technical papers, 8 book chapters and holds several patents in smart antennas and RF. He received "URSI Young Scientist Award" from International Union of Radio Science, 2002, "Japan Society of Promotion Science Fellowship Award", Japan, 2005, "Best Paper Award", LAPC, UK, 2012, etc. He has been a Principal Investigator for many projects including "Millimeter-wave intelligent array antennas for next-generation mobile satellite communications" (FLEXWIN, funded by European Union FP7 ICT Program), etc.

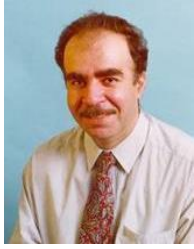


Anthony T.S. Ho (M'89-SM'94) received the B.Sc. (Hons) degree in physical electronics from Northumbria University, Newcastle upon Tyne, U.K., in 1979, the M.Sc. degree in applied optics from Imperial College London, London, U.K., in 1980, and the Ph.D. degree in digital image processing from King's College London, London, U.K., in 1983.

He holds a Personal Chair in Multimedia Security and has been Head of Department of Computing, University of Surrey, Surrey, U.K., since 2010. After graduation, he worked in industry for 11 years in the U.K. and Canada. From 1994 to 2005, he was a Senior Lecturer and then Associate Professor at Nanyang Technological University (NTU), Singapore. He has published more than 130 articles in international journals and conference proceedings as well as eight international patents granted related to watermarking

and steganography. He is the Editor-in-Chief of the international journal Information Security Technical Report published by Elsevier.

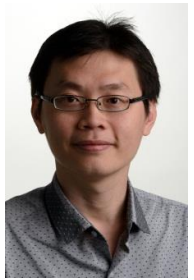
Prof. Ho is a Fellow of Institution of Engineering and Technology (FIET), Fellow of Institute of Physics (FInstP), and Fellow of British Computer Society (FBCS).



Raed A. Abd-Alhameed (M'11-SM'13) received the B.Sc. and M.Sc. degrees from Basrah University, Basrah, Iraq, in 1982 and 1985, respectively, and the Ph.D degree from the University of Bradford, West Yorkshire, UK, in 1997, all in electrical engineering.

He is a Professor of electromagnetic and radio frequency (RF) engineering in the School of Engineering, Design, and Technology at the University of Bradford, Bradford, U.K. He has over 20 years research experience in RF designs, antennas and electromagnetic computational techniques and has published over 400 academic journals and referred conference papers. He has led several funded projects from EPSRC, Health Department, Technology Strategy Board and Industry. His current research interests include hybrid electromagnetic, EMC, low SAR antennas, active antennas, beam steering antennas, MIMO antennas, RF predistorter including biological cell modeling for breast cancer applications.

Prof. Abd-Alhameed is the Fellow of the Institution of Engineering and Technology, Fellow of Higher Education Academy, and a Chartered Engineer. He is the Chair of several successful workshops on Energy Efficient and Reconfigurable Transceivers (EERT): Approach towards Energy Conservation and CO₂ Reduction that addresses the biggest challenges for the future wireless systems.



Chan H. See received a first class BEng Honours degree in Electronic, Telecommunication and Computer Engineering and a PhD degree from the University of Bradford, UK in 2002 and 2007 respectively. Currently, he is working as a senior research fellow in the Antennas and Applied Electromagnetics research group within the Electronics, Communications and Information Systems Engineering (ECISE), to support various projects related to sensors and antennas for the water industry. He has published over 100 journal articles and conference papers. He is a coauthor for 1 book and 1 book chapter.

He was a recipient of two Young Scientist Awards from International Union of Radio Science (URSI) and Asia-Pacific Radio Science Conference (AP-RASC) in 2008 and 2010 respectively. Dr See is a Chartered Engineer and Member of the Institution of Engineering and Technology (MIET). He has an NVQ level 4 in Management from the Chartered Management Institute.



Tim WC Brown (S'00-M'04) graduated from the University of Surrey in 1999 with a BEng in Electronic Engineering and since graduated with a PhD in antenna diversity for mobile terminals in the Centre for Communication Systems Research (CCSR) in 2004. Since completing his doctoral research, he has continued his research interests in antennas, propagation and radio frequency (RF) engineering. This has included postdoctoral research from 2004-2006 at Aalborg University, Denmark and his

present post as a lecturer in RF, antennas and propagation at CCSR. His current research interests include mobile terminal antennas, satellite communications, multiple input multiple output (MIMO), ultra wideband (UWB) radar, radio frequency identification (RFID), near field communications (NFC), vehicular technologies and future wireless.

Jianzhou Li received the B.E., M.E. and Ph.D. degrees from Northwestern Polytechnical University, China in 1995, 2002 and 2005, respectively. From 2008 to 2009, he was a visiting scholar at Surrey Space Centre, University of Surrey, UK. Currently he works as associate professor at School of Electronics and Information, Northwestern Polytechnical University, China. His research interests include computational electromagnetics and printed antennas.

Gao Wei was born in Shaanxi, China, in 1963. He received the Ph.D. degree from Northwestern Polytechnical University, Xi'an, China, in 2008. Currently, he is a professor at School of Electronics and Information, Northwestern Polytechnical University, China. His research interests include microwave measurement and microwave communication.

Jiadong Xu was born in Nanjing, China, in 1948. He received the M.Sc. degree from Northwestern Polytechnical University, Xi'an, China, 1981. Since 1990, he has been with School of Electronics and Information, Northwestern Polytechnical University, China, as a full professor working on antenna design, EM scattering theory and microwave measurement.